Geophysical Research Letters

RESEARCH LETTER
10.1029/2024GL109141

Phytoplankton Spring Bloom Inhibited by Marine Heatwaves in the North-Western Mediterranean Sea

Mengyu Li[1,2], Emanuele Organelli[2], Federico Serva[2], Marco Bellacicco[2], Angela Landolfi[2], Andrea Pisano[2], Salvatore Marullo[2], Fang Shen[1], Alexandre Mignot[3], Simon van Gennip[3], and Rosalia Santoleri[2]

[1]East China Normal University, State Key Laboratory of Estuarine and Coastal Research, Shanghai, China, [2]National Research Council of Italy (CNR), Institute of Marine Sciences (ISMAR), Rome, Italy, [3]Mercator Ocean International, Toulouse, France

Abstract Marine heatwaves (MHWs) represent anomalously warm temperature conditions of seawater that may affect marine life and ocean biogeochemistry. Under such conditions, phytoplankton communities may modify their structure and functions, and their resilience is not assured. This study characterizes the impact of MHWs on the phytoplankton spring bloom in the North-Western Mediterranean Sea. Here, we synergistically combine autonomous observations from BioGeoChemical-Argo floats, satellite-based and marine ecosystem model data, and show that MHW events occurring during winter drastically inhibit phytoplankton carbon biomass in spring by up to 70%. Such reduction is related to the enhanced stratification of the water column under MHWs which hinders the renewal of nutrients from deep-ocean reservoirs, thus preventing surface phytoplankton from blooming. This process negatively impacts particulate organic carbon stocks within the mixed layer, while severe events cause an earlier shift of phytoplankton phenology that provokes changes in zooplankton biomass distribution.

Plain Language Summary Marine heatwaves (MHWs) are described as an abnormal and prolonged increase of ocean temperatures. These events may occur in all the oceans, and are becoming more frequent than before. Such increase in water temperature might not be tolerated by organisms, which must need to adapt themselves to the new environmental conditions. Consequently, marine ecosystem health is endangered. Here, we analyze the effect that MHWs have on the growth of small algae called phytoplankton. Phytoplankton are vital microscopic organisms for ecosystems that use sunlight to produce organic carbon through photosynthesis. At middle and high latitudes, phytoplankton massively grows (i.e., blooms) once a year at the sea surface, and introduces a major carbon flux into the ecosystem that sustains larger animals. Through combining observations acquired by different platforms (satellites, autonomous in situ BioGeoChemical-Argo robots, and ecosystem models), we comprehensively study how MHWs affect phytoplankton carbon production during spring blooms and trophic chains at mid-latitudes. Results show that MHW events occurring in winter lead to a large decrease in phytoplankton carbon biomass (up to 70%) in spring. Winter MHW events, driven by local atmospheric conditions, intensify water column stratification thus hindering the deep-ocean nutrient transport to the surface, which is essential for phytoplankton to bloom.

Mengyu Li and Emanuele Organelli contributed equally to this work.

Key Points:

- Marine heatwaves (MHWs) intensify water stratification leading to reduction in nutrient supply which inhibits surface phytoplankton spring bloom
- MHWs lead to a phytoplankton community shift toward smaller cells, while increasing the transparency of surface waters
- MHWs decrease carbon stocks within the mixed layer, while intense ones shift phytoplankton phenology and affect zooplankton

Supporting Information:

Supporting Information may be found in the online version of this article.

Correspondence to:

E. Organelli,
emanuele.organelli@cnr.it

Citation:

Li, M., Organelli, E., Serva, F., Bellacicco, M., Landolfi, A., Pisano, A., et al. (2024). Phytoplankton spring bloom inhibited by marine heatwaves in the North-Western Mediterranean Sea. *Geophysical Research Letters*, *51*, e2024GL109141. https://doi.org/10.1029/2024GL109141

Received 5 MAR 2024
Accepted 25 AUG 2024

1. Introduction

Marine heatwaves (MHWs) are extreme events characterized by prolonged and anomalous warm ocean temperatures that profoundly impact the health of marine ecosystems (Hobday et al., 2016; Oliver et al., 2021). The occurrence of MHWs is increasing worldwide (Frölicher et al., 2018; Jacox et al., 2020), and the exposure of marine ecosystems to extreme variations in temperatures may change physiological adaptation, population and ecosystem structures (Smale et al., 2019), both at the ocean surface and at depth (Fragkopoulou et al., 2023). Currently, ecological responses to prominent MHW events have been observed across different spatio-temporal scales, including irreversible losses of species (Smith et al., 2023), fisheries (Cheung et al., 2021), and foundational habitats like seagrasses (Thomson et al., 2015), coral reefs (Hughes et al., 2019) and kelp forests (Wernberg et al., 2016).

Marine phytoplankton, which injects energy in the marine food web via photosynthesis, is also impacted by MHWs (Gruber et al., 2021; Le Grix et al., 2021). MHWs alter phytoplankton community function and structure (Long et al., 2021; Wyatt et al., 2022), leading to significant losses of marine productivity (Rodrigues et al., 2019;

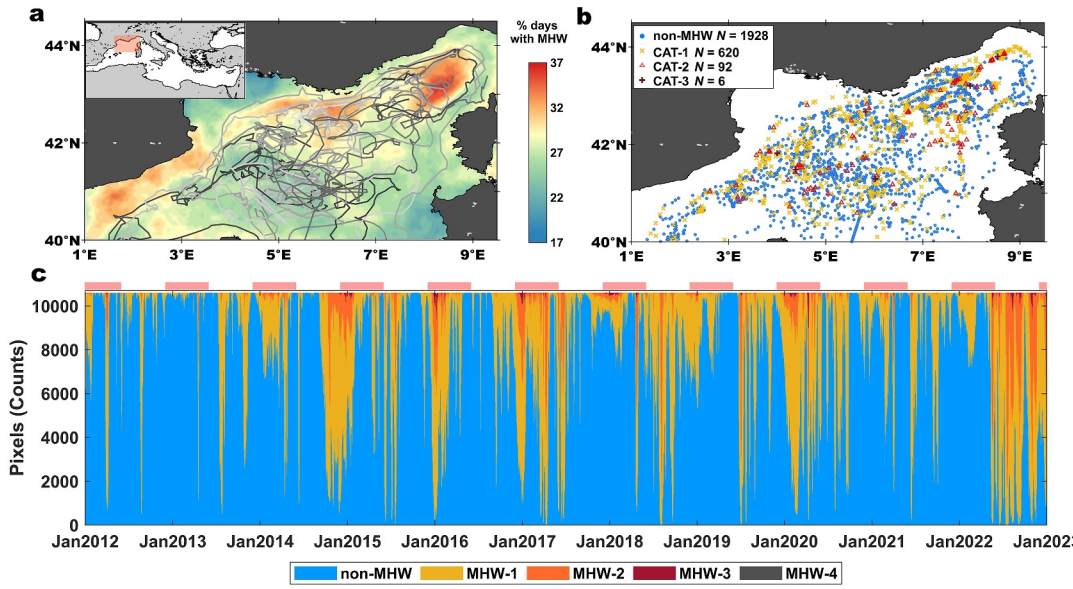

Figure 1. The North-Western Mediterranean Sea (NWM). (a) The 23 BioGeoChemical-Argo quality-controlled trajectories superimposed to percent days with Marine heatwaves (MHWs) for the period 2012–2022; (b) Float profiles (N = 2,646) grouped according to MHW categories. The blue dots represent profiles without MHWs. The yellow crosses, orange triangle and dark red plus-signs represent MHW categories 1, 2, and 3, respectively. (c) MHWs distribution in the NWM during 2012–2022 as derived from the MHW Atlas (Section 2.1). The light red shadows at the top represent the periods from December to May, which correspond to the months when the spring bloom is triggered and develops. Blue indicates the number of pixels without MHWs, while yellow, orange, red, and dark gray represent the number of pixels of MHWs classified as categories 1–4, respectively.

Smale et al., 2019). Phytoplankton massively grows (i.e., blooms) once a year at high and middle latitudes. At mid-latitudes, in the Mediterranean Sea, a phytoplankton bloom is only observed at the sea surface during spring in the northwestern region, where deep or intermediate water convection occurs (D'Ortenzio & Ribera d'Alcalà, 2009; Mignot et al., 2014; Sammartino et al., 2015; Santoleri et al., 2003; Volpe et al., 2012). Winter winds combined with autumn de-stratification of the water column modulate the intensity of the deep convection, and thus the enrichment of nutrients at the surface which eventually triggers the growth of large phytoplankton cells such as micro-planktonic diatoms (Marty et al., 2002; Mayot et al., 2017). Hence, winter MHWs occurring in this region are expected to have significant impacts on the vertical mixing and phytoplankton biomass increase, and finally on the regional carbon cycle (Mignot et al., 2018).

Here we showcase the impact of MHWs on the bloom of pelagic phytoplankton communities at the surface of the offshore productive waters of the North-Western Mediterranean Sea (NWM). This region is indeed characterized by an intense warming trend (Pisano et al., 2020) which brings to prolonged and recurrent MHW events mostly within the uppermost 200 m (Juza et al., 2022; Martínez et al., 2023; Marullo et al., 2023). Synergistically combining in situ vertical profiles from autonomous BioGeoChemical-Argo (BGC-Argo) floats with space-borne observations, we show that winter MHW events limit the phytoplankton growth in spring between the years 2012 and 2022. Given MHW's persistency from winter to spring and their frequency over the examined years in NWM (Figure 1), we first discuss average conditions of phytoplankton productivity and ecosystem biogeochemical status for MHWs against non-MHW conditions within the mixed layer, as derived from profiles acquired by several BGC-Argo floats. We then use satellite-derived measurements of the ocean color to corroborate results from in situ observations for the whole NWM. Finally, we showcase the impact of MHWs of different intensities on the spring phytoplankton biomass bloom and particulate organic carbon (POC) pools based on observations of a single BGC-Argo float, and on co-located model-derived zooplankton biomass distribution.

2. Materials and Methods

2.1. Marine Heatwaves Atlas

The daily record of MHWs in the NWM (40°–45°N, 1°–10°E) was obtained by applying the methodology of Hobday et al. (2016, 2018) to Sea Surface Temperature (SST) data for the period 1982–2022. Specifically, Mediterranean SSTs were extracted from the global daily European Space Agency (ESA) Climate Change Initiative (CCI) SST product (version 2) on 0.05° × 0.05° grid (Merchant et al., 2019). The CCI data set was obtained from satellite thermal infrared measurements by the Advanced Very High Resolution Radiometers, the Along-Track Scanning Radiometers series, and the Sentinel-3's Sea and Land Surface Temperature Radiometer. The MHW detection algorithm was then applied to native resolution data using the period 1985–2012 as baseline to calculate the 90th percentile threshold, with an 11-day smoothing window (Hobday et al., 2018). Each day and pixel were assigned to a given MHW category (between 0, no heatwave and 4, extreme heatwave) depending on the local SSTs, following Hobday et al. (2016, 2018).

2.2. In Situ BGC-Argo Data Set

An array of 23 BGC-Argo floats distributed in the research area was obtained from the Coriolis database (last access: 19 January 2023), and included 2,646 vertical profiles collected between 0 and 1,000 m from 24 November 2012 to 31 December 2022, every 1 up to 10 days (Figure 1a). The BGC-Argo profiles were matched with the MHW Atlas by selecting the corresponding sampling date and nearest pixel available. The number of profiles associated with MHWs of categories 1 to 3 were 620, 92, and 6, respectively (Figure 1b). No matches with MHWs of category 4 were found. The analysis of MHW occurrence between 2012 and 2022 confirmed that MHWs in the NWM are frequent in winter and persist into the following spring (Figure 1c).

All the BGC-Argo floats were deployed according to standard procedures (Bittig et al., 2019; Stoer et al., 2023). Pressure (dbar), temperature (T, °C), and salinity (S, PSU) were collected by the SBE-41CP conductivity-T-depth sensor (Sea-Bird Scientific) and quality-controlled (Wong et al., 2023). Seawater density was calculated following the UNESCO polynomial equation (Fofonoff & Millard, 1983). The mixed layer depth (MLD, m) was computed as the depth where the density was higher than its value at 10 m by 0.03 kg m^{-3} (de Boyer Montégut et al., 2004). Water column stratification was quantified by the square of buoyancy frequency (N^2, s^{-2}) following Li et al. (2020). Chlorophyll-*a* fluorescence and the angular scattering function at 700 nm were acquired with an ECO Puck triplet (Sea-Bird Scientific), then converted to chlorophyll-*a* concentration (Chl*a*, mg m^{-3}) and optical particle backscattering coefficient at 700 nm ($b_{bp}(700)$, m^{-1}). Negative and invalid values were eliminated both for Chl*a* and $b_{bp}(700)$, while abnormal high-deep-water values were removed only for Chl*a* (Schmechtig, Claustre, et al., 2018; Schmechtig, Poteau, et al., 2018). Photosynthetically Available Radiation (PAR, µmol quanta m^{-2} s^{-1}) was acquired by an OCR-504 radiometer (Sea-Bird Scientific) and quality-controlled for environmental perturbations (Organelli et al., 2016). The depth of the euphotic zone (z_{eu}, m), defined as 1% of its value just below the sea surface, was obtained from quality-controlled PAR following Organelli, Barbieux, et al. (2017). Nitrate concentration (mmol m^{-3}) measured by SUNA V2 sensors (Sea-Bird Scientific) carried by 8 floats were quality-controlled following Johnson et al. (2023). All variables with quality Flags 1 and 2 were saved, as well as Flag 5 for Chl*a* (Carval et al., 2022).

Additional quantities from quality-controlled BGC-Argo optical variables, such as the concentration of phytoplankton carbon (C_{phyto}, mg C m^{-3}) used as the proxy of phytoplankton biomass, net primary production (NPP, mg C m^{-3} d^{-1}) and the concentration of POC (mg C m^{-3}) were computed. C_{phyto}, described as $SF[b_{bp}(700) - b^{k}_{bp}(700)]$, was obtained from the b_{bp}-based model by Behrenfeld et al. (2005), using a scaling factor of 16,455 mg C m^{-2} and monthly non-algal particles b_{bp} coefficients (b^{k}_{bp}, m^{-1}) at 700 nm tailored for the NWM (Bellacicco, Cornec, et al., 2019; Bellacicco, Vellucci, et al., 2019). NPP was estimated from C_{phyto}, Chl*a* and PAR following the carbon-based productivity model designed for BGC-Argo applications (Arteaga et al., 2022).

Depth-integrated values of Chl*a*, C_{phyto}, and NPP within the mixed layer were computed (hereafter named as $iChla_{MLD}$, iC_{phyto_MLD}, and $iNPP_{MLD}$, respectively). MLD-integrated values referring to MHW conditions were compared against non-MHW states by the Wilcoxon rank-sum test.

10.1029/2024GL109141

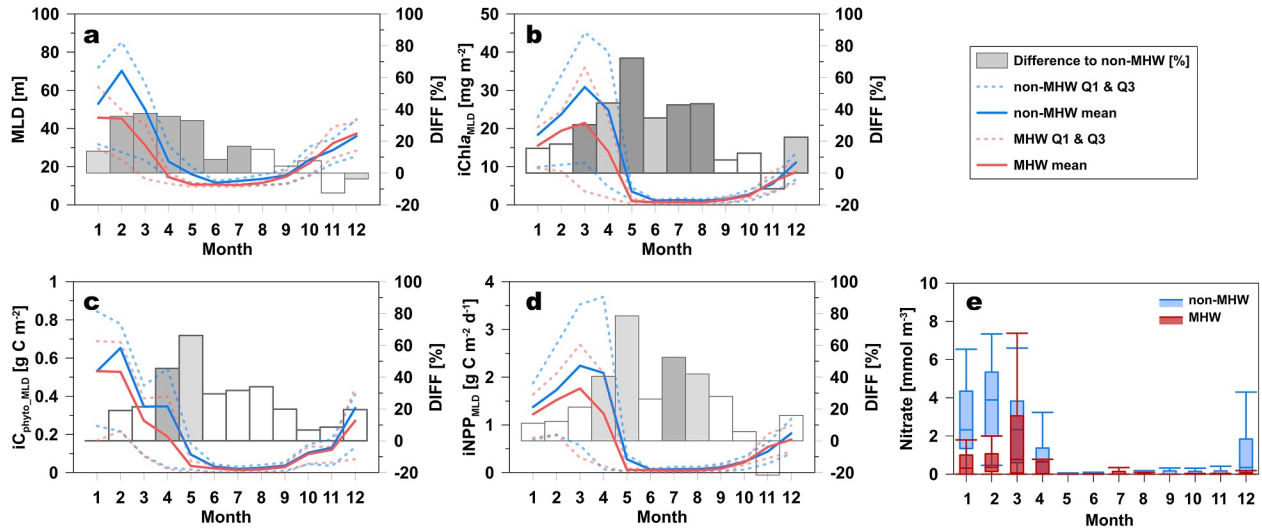

Figure 2. (a) Average mixed layer depth (MLD), (b) iChla$_{MLD}$, (c) iC$_{phyto_MLD}$, (d) iNPP$_{MLD}$, and (e) average nitrate concentrations within mixed layer with and without Marine heatwave (MHW) events, computed by binning monthly BioGeoChemical-Argo profile measurements from 2012 to 2022. In panels (a–d), bars represent differences between MHW and non-MHW conditions. White bars represent $p > 0.05$ in the Wilcoxon test; Light gray bars indicate $p < 0.05$; Dark gray bars represent $p < 0.01$. The solid blue lines represent mean values under non-MHW conditions, while the solid red lines represent mean values under MHW conditions. Dashed lines represent upper and lower quartiles.

POC was calculated from BGC-Argo measured and quality-controlled profiles of $b_{bp}(700)$ and Chl*a* following the multivariable empirical algorithm described by Model B parametrized for wavelength of 700 nm in Koestner et al. (2022). Then, carbon stocks were computed by integrating each POC profile within the mixed layer.

2.3. Ocean Color Data Set

Monthly remote sensing reflectance spectra (R_{rs}, sr^{-1}) with 4-km resolution were downloaded from the GlobColour archive released in the framework of the European Copernicus Marine Service for the period 2012–2022. R_{rs} spectra represented the merged product of SeaWiFS, MODIS, MERIS, VIIRS, Sentinel-3's OLCI satellite sensors (Colella et al., 2023), at 412, 443, 490, 555, and 670 nm. The phytoplankton size classes (PSC) were derived from the Copernicus Marine GlobColour R_{rs} by a globally tuned spectral-based approach and expressed as the fraction of micro-, nano-, and pico-phytoplankton size classes relative to the total chlorophyll-*a* concentration (Xi et al., 2020, 2021). The PSC uncertainties are reported in Xi et al. (2021) and Garnesson et al. (2023). The Chi-square test was used to check significance of PSC distributions differences with and without MHWs.

2.4. Zooplankton Biomass Data Set

Daily depth-integrated zooplankton biomass mass content in the epipelagic layer (iZooc, g C m^{-2}) was obtained on a 0.083° × 0.083° grid, for the period 2019–2020, from the Spatial Ecosystem And POpulation DYnamic Model (SEAPODYM) (Lehodey et al., 2010, 2015) through the European Copernicus Marine Service. The model is forced by ocean currents, temperature, and NPP (Titaud, Conchon, & Mérillet, 2023), with NPP as the dominant input. Zooplankton biomass is modeled as a single functional group only in the epipelagic layer, determined as the 1.5 times z_{eu} (Lehodey et al., 2010, 2015). A comparison of z_{eu} and NPP integrated within z_e between SEAPODYM and calculated from a single co-located BGC-Argo float (WMO 7900562) is shown in Figure S1 in Supporting Information S1. Zooplankton ranges from 0.2 to 20 mm (e.g., vertically migrating copepods, meroplanktonic larvae), thus bridging between phytoplankton and higher trophic levels. Further details on the zooplankton product validation can be found in the quality information report of the product (Titaud, Conchon, Mérillet, & Goeman, 2023).

3. Results and Discussion

During winter, in the NWM, the analysis of BGC-Argo data averaged from 2012 to 2022 shows that MHWs result in a significant reduction of the MLD of about 50% (Figure 2a), which is followed by a sharp decline of the

phytoplankton biomass in spring. When comparing average MHW against non-MHW conditions, depth-integrated Chl*a* (iChla_{MLD}) within the MLD reaches a maximum decline of 70% in May (Figure 2b and Figure S2 in Supporting Information S1 for profiles). However, iChla_{MLD} significantly decreases with MHWs also in summer when phytoplankton biomass is expected to be close to zero (Figure 2b). Hence, while Chl*a* variations in spring might be more correlated to actual changes in biomass, changes in summer are most likely related to a physiological adaptation of phytoplankton communities (Bellacicco et al., 2016). Such results thus suggest that Chl*a* alone cannot be used as a robust proxy to study MHW-related impacts on phytoplankton biomass and ecosystem productivity.

Phytoplankton carbon (iC_{phyto_MLD}) instead reveals substantial declines under MHW conditions only in spring, with 50% and 70% reductions of iC_{phyto_MLD} in April and May, respectively (Figure 2c and Figure S3 in Supporting Information S1 for profiles). Such decreases are further accompanied by an approximately 40%–80% decrease in iNPP_{MLD} during the same months (Figure 2d and Figure S4 in Supporting Information S1 for profiles). Indeed, when MHWs occur, due to favorable atmospheric conditions (Marullo et al., 2023), the significantly shallower MLD leads to an 80% decline in surface nitrate concentrations in winter (Figure 2e and Figure S5 in Supporting Information S1 for profiles). Thus, if new nutrients cannot be injected into the upper layer of the ocean from the deep reservoirs due to increased stratification of the water column, the large and productive phytoplankton fail to grow at the surface (Arteaga & Rousseaux, 2023; Morán et al., 2010; Trainer et al., 2020; Wyatt et al., 2022). The weaker nutrient replenishment at the surface caused by MHWs is then followed by nutrient rapid depletion because the sustained temperature likely increases the phytoplankton respiration, cell metabolism, and nutrient consumption capacity (Soulié et al., 2022). Besides the impact of nutrient decline on iC_{phyto_MLD} due to MLD shallowing, significant changes in Chl*a* and C_{phyto} are observed propagated down to z_{eu} in April and May that can also be explained by vertical nutrient declines with MHWs (Figures S5 and S6 in Supporting Information S1).

In situ temperature (T) and the squared buoyancy frequency (N^2; high N^2 are associated with vertical stratification) profiles during MHW events serve as direct evidence of the increased vertical stratification in winter (Figure 3 and Figure S7 in Supporting Information S1 for T and N^2 profiles). MHW events in December and January are characterized by positive thermal anomalies of 2°C on average in the upper layer (Figures 3a and 3b), which provoke an intensification of the thermocline magnitude accompanied by significant increases in N^2 down to ∼200 m depth (Figures 3g and 3h). During these months, MHWs of category 2 and 3 increase stratification up to 70–80 m deeper than MHWs of category 1 (Figures 3g–3i). In spring, increases of stratification due to MHWs are mainly observed within the first 40 m, while a similar behavior to normal T and N^2 conditions is observed below (Figures 3d–3f and 3j–3l). In autumn, MHWs help extend summer stratification further suppressing the expected vertical mixing in the cold seasons (Figure S8 in Supporting Information S1). Our results thus confirm that the MHW vertical propagations in the NWM is primarily confined to ∼200 m depth, while MHWs impacts is mainly concentrated in the upper layer (Juza et al., 2022; Köhn et al., 2024; Zhang et al., 2023).

To extend the analysis across the entire period and NWM area, we analyze remote sensing ocean color data (Figure 4). Spectral remote-sensing data under MHW conditions show a tendency to increase in the blue spectral region from March to May when the phytoplankton bloom is expected to occur. The increase at 412 and 443 nm during winter is less than 10% compared with non-MHWs (Figures 4a–4c), while the average R_{rs}(412) and R_{rs}(443) significantly rises by 20% in April and May (Figures 4e and 4f). Besides reduction in phytoplankton biomass, such shift to bluer waters can also be related to the shift from micro- and nano-phytoplankton to pico-phytoplankton (Figure 4g). The micro-phytoplanktonic diatoms that generally dominate the spring bloom in NWM (Sammartino et al., 2015) and cause high primary productivity (Bricaud et al., 2002; Uitz et al., 2012), contain high Chl*a* and other light harvesting pigments that absorb from blue to green bands of the visible light (Organelli, Nuccio, et al., 2017). Although considering the high uncertainty of satellite-derived PSC product, which can reach the maximum median percent difference of 56.25% for 6 phytoplankton classes (Xi et al., 2021), a chi-square test confirms a significant shift from micro- to pico-phytoplankton (Figure 4g). The observed phytoplankton community shift is consistent with waters where blue light is more available (Organelli et al., 2021), which finally reflects the observed spectral modifications of R_{rs} in the blue and therefore translates into an increased transparency of the water when MHWs occur.

Using a single BGC-Argo float we finally examine the impact of MHWs of different intensities on the phytoplankton bloom and POC stocks within the mixed layer in the NWM (Figure 5). Float WMO 7900562

10.1029/2024GL109141

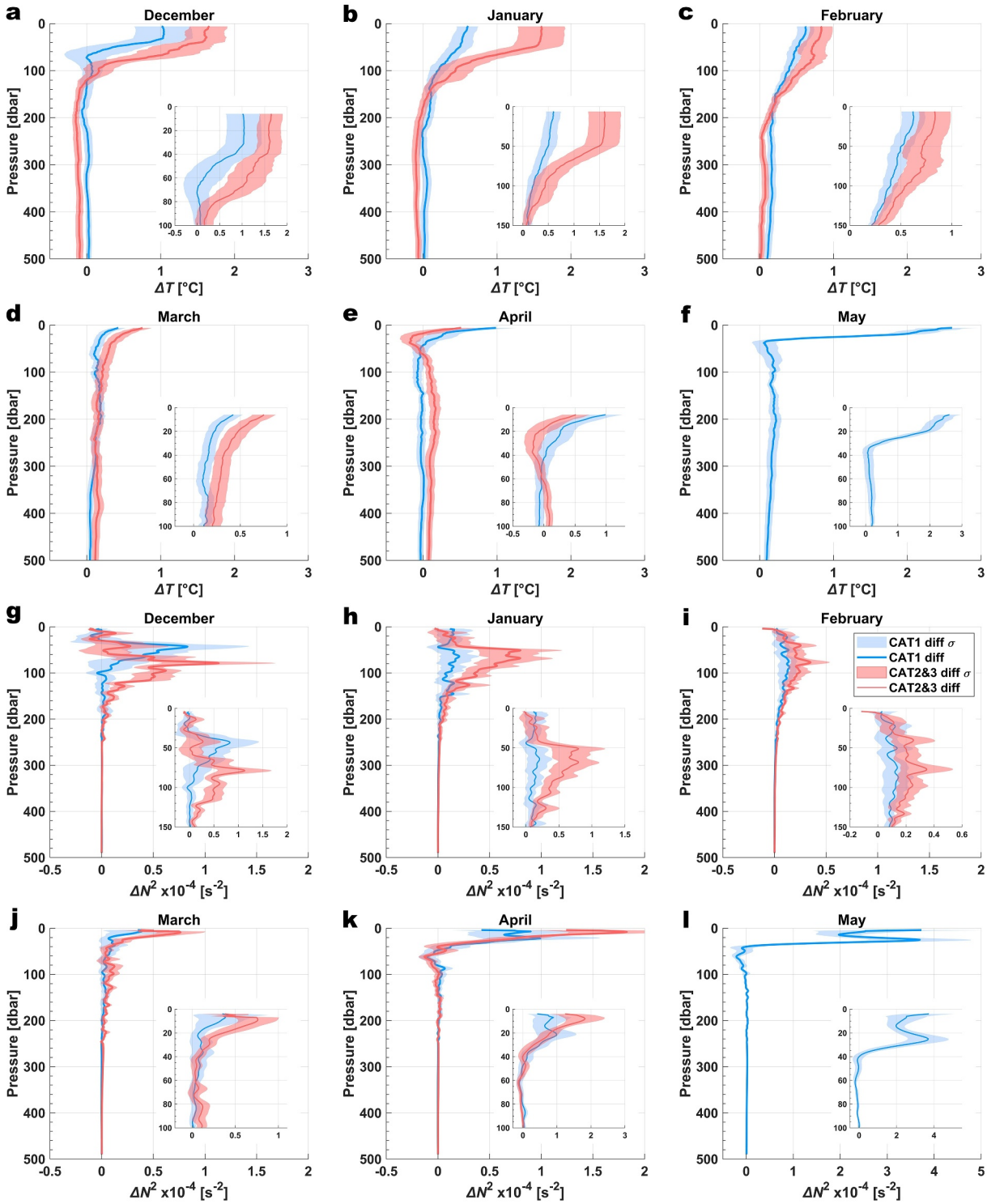

Figure 3. The average difference of BioGeoChemical-Argo temperature, T (a–f) and squared buoyancy frequency, N^2 (g–i) under Marine heatwaves (MHWs) to non-MHW conditions, grouped into MHW categories from December to May, over the period 2012–2022. The blue and red lines represent the difference between MHW category 1 and category 2 plus 3 profiles to non-MHW conditions, respectively. Small figures are detailed views of the upper 100–150 m. The red and blue shadows represent the standard deviations σ.

10.1029/2024GL109141

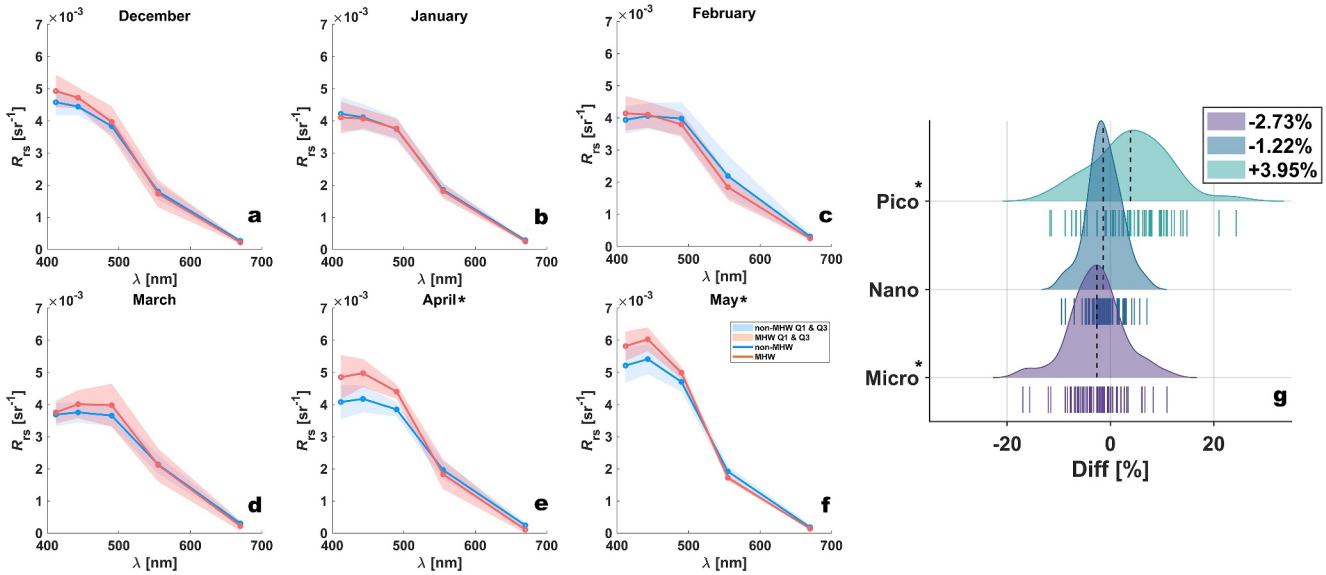

Figure 4. (a–f) Monthly $R_{rs}(\lambda)$ spectra grouped into Marine heatwave (MHW) (red lines) and non-MHW (blue lines) conditions for the North-Western Mediterranean Sea basin. Red and blue shadows are the standard deviations. * represents Wilcoxon test $p < 0.05$ for the blue bands. (g) Monthly distribution of the phytoplankton size classes mass concentration percentage difference between MHW and non-MHW conditions for the period 2012–2022, * represents Chi-square test $p < 0.05$. The dash lines are the average, the lines below represent the actual differences between MHW and non-MHW values.

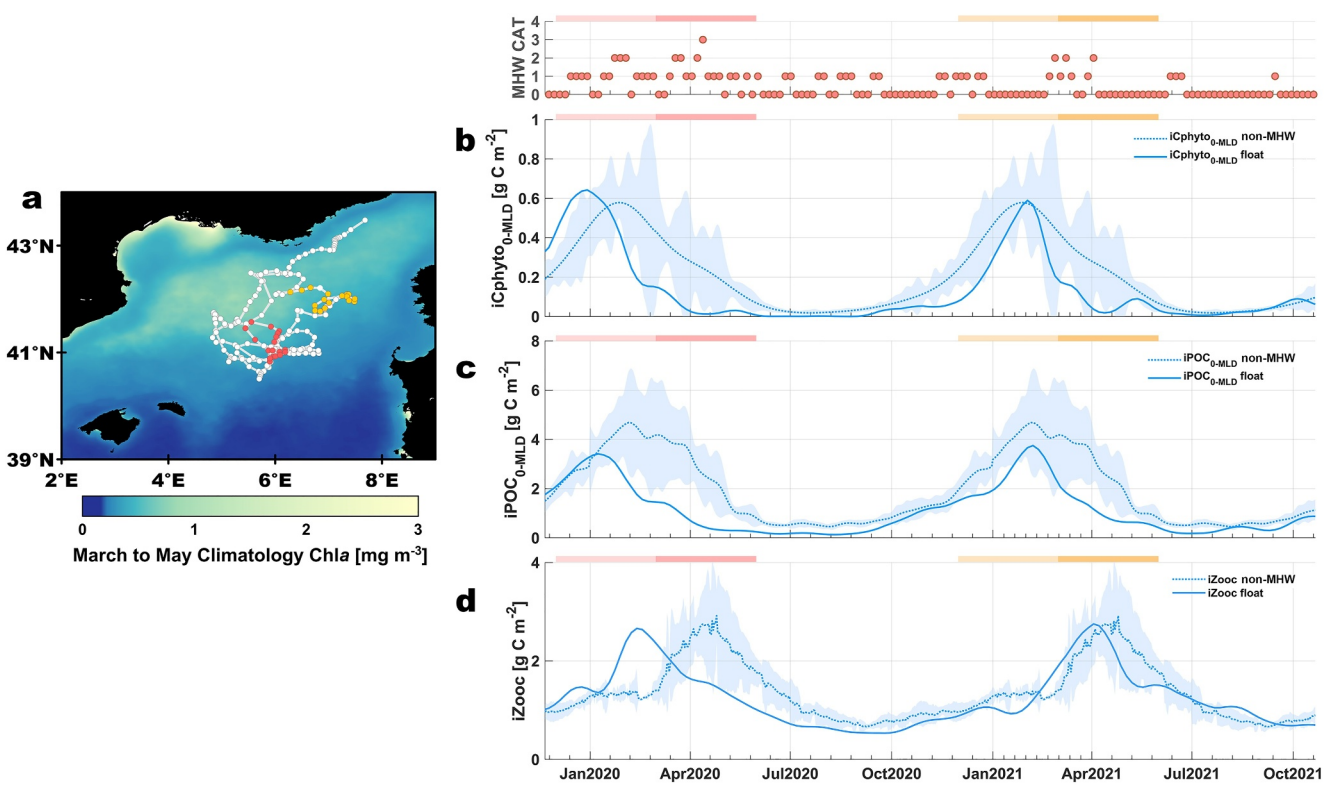

Figure 5. (a) March to May averaged climatology Chl*a* map over the North-Western Mediterranean Sea, with the trajectory of float WMO 7900562. The red, yellow, and white dots represent the profiles in spring of 2020 (more intense Marine heatwaves (MHWs)), 2021 (less intense MHWs), and other conditions, respectively. (b) BioGeoChemical (BGC)-Argo derived C_{phyto} stock within the mixed layer ($iCphyto_{0–MLD}$), and regional non-MHW average; (c) BGC-Argo derived particulate organic carbon stock within the mixed layer ($iPOC_{0–MLD}$), and regional non-MHW average. (d) Model-derived zooplankton biomass within epipelagic layer (iZooc) and non-MHW average. In panels (b–d) the regional non-MHW averages are computed by daily binning. Co-located MHW categories are shown at the top, red and yellow bars indicate the spring of 2020 (more intense MHWs) and 2021 (less intense MHWs), respectively. Light shadings represent winter.

encountered, from winter to spring, more intense (up to category 3) MHWs and less intense (up to category 2) MHWs in 2020 and 2021, respectively. During the more intense MHW in 2020, the biomass peak in terms of C_{phyto} shifts 1 month earlier compared to non-MHW conditions, and spring phytoplankton carbon significant decreases by over 90% (Figure 5b). Under such severe conditions, the POC stock peak within the mixed layer also occurs 1 month earlier, with a maximum decrease of 63.5% (Figure 5c). In winter 2021, under the less intense MHW event, the C_{phyto} maximum is not shifted in time, though a significant decrease of 80% is observed in spring compared to non-MHW conditions. A similar behavior is observed also for POC with a maximum decrease of 59.3%. As confirmed from BGC-Argo vertical profiles (Figures S3, S7, and S9 in Supporting Information S1), MHW events of varying intensities elicit different responses in vertical temperature increases and stratification, thus leading to distinct changes in phytoplankton phenology and biomass, as well as reduced carbon stocks in the upper layer that may ultimately reduce the efficacy of carbon export to the deep ocean (Cavan et al., 2019; Gao et al., 2021).

The impacts of MHWs propagate through the food chain, from primary producers to higher trophic levels, like zooplankton. Model-derived zooplankton biomass experiences a significant decrease in spring, with MHWs up to category 3 causing up to 50% biomass loss, and the peak shifting ~2 months earlier in response to the timing of the phytoplankton peak (Figures 5a and 5d). Under the less intense event in 2021, iZooc decreases only by 30% in spring with no significant phenological change compared to non-MHW conditions (Figure 5d). The altered zooplankton phenology and reduced biomass in the NWM could thus result from changes in food availability, as well as from increased temperatures due to MHWs, which enhance zooplankton respiration (Ratnarajah et al., 2023). Despite the complex structure of oceanic food webs, shifts in phytoplankton and zooplankton phenologies and biomass could lead to significant ecosystem consequences, including reduced fish recruitment and altered migration and spawning behaviors in the region (Feuilloley et al., 2020; Trainer et al., 2020).

4. Conclusions

Continuous in situ measurements from BGC-Argo floats in the NWM from 2012 to 2022, combined with satellite and model data, have revealed the inhibition of the annual spring phytoplankton bloom in response to MHW events. Main findings are:

- MHWs in winter significantly enhance the stratification of the water column and reduce the vertical mixing. Such conditions prevent nutrient renewal from deep sea reservoirs that ultimately leads to a significant reduction of phytoplankton carbon biomass (up to 70%) and of NPP (80%) within the mixed layer in spring.
- The reduction in phytoplankton biomass and the shift toward smaller cells in response to MHWs leads to increased water transparency.
- Compared to less intense MHW events, MHWs up to category 3 result in 1-month and 2-month earlier shifts of phytoplankton and zooplankton biomass, respectively. POC stocks are also reduced under MHWs.

While MHWs tend to increase in frequency and duration in the NWM (Marullo et al., 2023), the rapid and abnormal depletion of nutrients could lead to a decline in regional water productivity toward persistent oligotrophication (Leonelli et al., 2022). Reduced carbon stocks within the upper layer and smaller phytoplankton sizes potentially diminish the energy source to support deep-water ecosystems, which may trigger cascading effects on the entire ecosystem of the area (Trainer et al., 2020). This implies that pelagic ecosystems strongly affected by MHWs might not provide ecosystem-based services anymore such as carbon transfer and support to higher trophic levels.

Conflict of Interest

The authors declare no conflicts of interest relevant to this study.

Data Availability Statement

BGC-Argo data were collected and made freely available by the International Argo Program and the national programs that contribute to it (Argo, 2023). The Argo Program is part of the Global Ocean Observing System (GOOS). The ESA-CCI daily SST data set is available from the Copernicus Climate Change Service (Copernicus Climate Change Service, 2019). The monthly GlobColour R_{rs} at 4 km resolution and PSC products are freely

available from the Copernicus Marine Service (Copernicus Marine Service, 2023a). The daily epipelagic zooplankton biomass is freely available from the Copernicus Marine Global Ocean Low and Mid Trophic Levels Biomass Content Hindcast Product (Copernicus Marine Service, 2023b).

Acknowledgments
We are grateful for the constructive comments from the anonymous reviewers. This work has been supported by the "CAREHeat—deteCtion and threAts of maRinE Heat waves" project, funded by the European Space Agency—ESA (Contract 4000137121/21/I-DT). Mengyu Li acknowledges the China Scholarship Council (Grant 202206140082) for the joint PhD-program in CNR-ISMAR (Rome, Italy). Fang Shen is supported by the National Natural Science Foundation of China (42076187) and Science & Technology Commission of Shanghai Municipality (23590780200).

References

Argo. (2023). Argo float data and metadata from Global Data Assembly Centre (Argo GDAC) [Dataset]. *SEANOE*. https://doi.org/10.17882/42182

Arteaga, L. A., Behrenfeld, M. J., Boss, E., & Westberry, T. K. (2022). Vertical structure in phytoplankton growth and productivity inferred from biogeochemical-Argo floats and the carbon-based productivity model. *Global Biogeochemical Cycles*, *36*(8), e2022GB007389. https://doi.org/10.1029/2022GB007389

Arteaga, L. A., & Rousseaux, C. S. (2023). Impact of Pacific Ocean heatwaves on phytoplankton community composition. *Communications Biology*, *6*(1), 263. https://doi.org/10.1038/s42003-023-04645-0

Behrenfeld, M. J., Boss, E., Siegel, D. A., & Shea, D. M. (2005). Carbon-based ocean productivity and phytoplankton physiology from space. *Global Biogeochemical Cycles*, *19*(1), GB1006. https://doi.org/10.1029/2004GB002299

Bellacicco, M., Cornec, M., Organelli, E., Brewin, R. J. W., Neukermans, G., Volpe, G., et al. (2019). Global variability of optical backscattering by non-algal particles from a biogeochemical-Argo data set. *Geophysical Research Letters*, *46*(16), 9767–9776. https://doi.org/10.1029/2019gl084078

Bellacicco, M., Vellucci, V., Scardi, M., Barbieux, M., Marullo, S., & D'Ortenzio, F. (2019). Quantifying the impact of linear regression model in deriving bio-optical relationships: The implications on ocean carbon estimations. *Sensors*, *19*(13), 3032. https://doi.org/10.3390/s19133032

Bellacicco, M., Volpe, G., Colella, S., Pitarch, J., & Santoleri, R. (2016). Influence of photoacclimation on the phytoplankton seasonal cycle in the Mediterranean Sea as seen by satellite. *Remote Sensing of Environment*, *184*, 595–604. https://doi.org/10.1016/j.rse.2016.08.004

Bittig, H. C., Maurer, T. L., Plant, J. N., Schmechtig, C., Wong, A. P., Claustre, H., et al. (2019). A BGC-Argo guide: Planning, deployment, data handling and usage. *Frontiers in Marine Science*, *6*, 502. https://doi.org/10.3389/fmars.2019.00502

Bricaud, A., Bosc, E., & Antoine, D. (2002). Algal biomass and sea surface temperature in the Mediterranean Basin: Intercomparison of data from various satellite sensors, and implications for primary production estimates. *Remote Sensing of Environment*, *81*(2–3), 163–178. https://doi.org/10.1016/S0034-4257(01)00335-2

Carval, T., Keeley, R., Takatsuki, Y., Yoshida, T., Loch, S., Schmid, C., et al. (2022). Argo user's manual. https://doi.org/10.13155/29825

Cavan, E. L., Henson, S. A., & Boyd, P. W. (2019). The sensitivity of subsurface microbes to ocean warming accentuates future declines in particulate carbon export. *Frontiers in Ecology and Evolution*, *6*, 230. https://doi.org/10.3389/fevo.2018.00230

Cheung, W. W., Frölicher, T. L., Lam, V. W., Oyinlola, M. A., Reygondeau, G., Sumaila, U. R., et al. (2021). Marine high temperature extremes amplify the impacts of climate change on fish and fisheries. *Science Advances*, *7*(40), eabh0895. https://doi.org/10.1126/sciadv.abh0895

Colella, S., Böhm, E., Cesarini, C., Garnesson, P., Netting, J., & Calton, B. (2023). *Copernicus marine product user manual: For ocean colour products*. EU Copernicus Marine Service. https://doi.org/10.48670/moi-00281

Copernicus Climate Change Service. (2019). Sea surface temperature daily data from 1981 to present derived from satellite observations [Dataset]. *Copernicus Climate Change Service (C3S) Climate Data Store (CDS)*. https://doi.org/10.24381/cds.cf608234

Copernicus Marine Service. (2023a). Global ocean colour (Copernicus-GlobColour), bio-geo-chemical, L4 (monthly and interpolated) from satellite observations (1997-ongoing) [Dataset]. *Copernicus Marine Product Information*. https://doi.org/10.48670/moi-00281

Copernicus Marine Service. (2023b). Global ocean low and mid trophic levels biomass content hindcast [Dataset]. *Copernicus Marine Product Information*. https://doi.org/10.48670/moi-00020

de Boyer Montégut, C., Madec, G., Fischer, A. S., Lazar, A., & Iudicone, D. (2004). Mixed layer depth over the global ocean: An examination of profile data and a profile-based climatology. *Journal of Geophysical Research*, *109*(C12), C12003. https://doi.org/10.1029/2004JC002378

D'Ortenzio, F., & Ribera d'Alcalà, M. (2009). On the trophic regimes of the Mediterranean Sea: A satellite analysis. *Biogeosciences*, *6*(2), 139–148. https://doi.org/10.5194/bg-6-139-2009

Feuilloley, G., Fromentin, J.-M., Stemmann, L., Demarcq, H., Estournel, C., & Saraux, C. (2020). Concomitant changes in the environment and small pelagic fish community of the Gulf of Lions. *Progress in Oceanography*, *186*, 102375. https://doi.org/10.1016/j.pocean.2020.102375

Fofonoff, N. P., & Millard, R., Jr. (1983). *Algorithms for the computation of fundamental properties of seawater*. UNESCO. https://doi.org/10.25607/OBP-1450

Fragkopoulou, E., Sen Gupta, A., Costello, M. J., Wernberg, T., Araújo, M. B., Serrão, E. A., et al. (2023). Marine biodiversity exposed to prolonged and intense subsurface heatwaves. *Nature Climate Change*, *13*(10), 1114–1121. https://doi.org/10.1038/s41558-023-01790-6

Frölicher, T. L., Fischer, E. M., & Gruber, N. (2018). Marine heatwaves under global warming. *Nature*, *560*(7718), 360–364. https://doi.org/10.1038/s41586-018-0383-9

Gao, G., Zhao, X., Jiang, M., & Gao, L. (2021). Impacts of marine heatwaves on algal structure and carbon sequestration in conjunction with ocean warming and acidification. *Frontiers in Marine Science*, *8*, 758651. https://doi.org/10.3389/fmars.2021.758651

Garnesson, P., Mangin, A., Bretagnon, M., & Jutard, Q. (2023). Global ocean colour (Copernicus-GlobColour), bio-geo-chemical, L4 (monthly and interpolated) from satellite observations (1997-ongoing) quality information document: EU Copernicus marine service. Retrieved from https://catalogue.marine.copernicus.eu/documents/QUID/CMEMS-OC-QUID-009-101to104-111-113-116-118.pdf

Gruber, N., Boyd, P. W., Frölicher, T. L., & Vogt, M. (2021). Biogeochemical extremes and compound events in the ocean. *Nature*, *600*(7889), 395–407. https://doi.org/10.1038/s41586-021-03981-7

Hobday, A. J., Alexander, L. V., Perkins, S. E., Smale, D. A., Straub, S. C., Oliver, E. C., et al. (2016). A hierarchical approach to defining marine heatwaves. *Progress in Oceanography*, *141*, 227–238. https://doi.org/10.1016/j.pocean.2015.12.014

Hobday, A. J., Oliver, E. C., Gupta, A. S., Benthuysen, J. A., Burrows, M. T., Donat, M. G., et al. (2018). Categorizing and naming marine heatwaves. *Oceanography*, *31*(2), 162–173. https://doi.org/10.5670/oceanog.2018.205

Hughes, T. P., Kerry, J. T., Connolly, S. R., Baird, A. H., Eakin, C. M., Heron, S. F., et al. (2019). Ecological memory modifies the cumulative impact of recurrent climate extremes. *Nature Climate Change*, *9*(1), 40–43. https://doi.org/10.1038/s41558-018-0351-2

Jacox, M. G., Alexander, M. A., Bograd, S. J., & Scott, J. D. (2020). Thermal displacement by marine heatwaves. *Nature*, *584*(7819), 82–86. https://doi.org/10.1038/s41586-020-2534-z

Johnson, K. S., Plant, J. N., Sakamoto, C., Maurer, T. L., Pasqueron, D. F. O., Serra, R., et al. (2023). Processing bio-Argo nitrate concentration at the DAC level [Report]. *Argo Data Management*. https://doi.org/10.13155/46121

Juza, M., Fernández-Mora, À., & Tintoré, J. (2022). Sub-regional marine heat waves in the Mediterranean Sea from observations: Long-term surface changes, sub-surface and coastal responses. *Frontiers in Marine Science*, *9*, 785771. https://doi.org/10.3389/fmars.2022.785771

Koestner, D., Stramski, D., & Reynolds, R. A. (2022). A multivariable empirical algorithm for estimating particulate organic carbon concentration in marine environments from optical backscattering and chlorophyll-a measurements. *Frontiers in Marine Science*, *9*, 941950. https://doi.org/10.3389/fmars.2022.941950

Köhn, E. E., Vogt, M., Münnich, M., & Gruber, N. (2024). On the vertical structure and propagation of marine heatwaves in the Eastern Pacific. *Journal of Geophysical Research: Oceans*, *129*(1), e2023JC020063. https://doi.org/10.1029/2023JC020063

Le Grix, N., Zscheischler, J., Laufkötter, C., Rousseaux, C. S., & Frölicher, T. L. (2021). Compound high-temperature and low-chlorophyll extremes in the ocean over the satellite period. *Biogeosciences*, *18*(6), 2119–2137. https://doi.org/10.5194/bg-18-2119-2021

Lehodey, P., Conchon, A., Senina, I., Domokos, R., Calmettes, B., Jouanno, J., et al. (2015). Optimization of a micronekton model with acoustic data. *ICES Journal of Marine Science*, *72*(5), 1399–1412. https://doi.org/10.1093/icesjms/fsu233

Lehodey, P., Murtugudde, R., & Senina, I. (2010). Bridging the gap from ocean models to population dynamics of large marine predators: A model of mid-trophic functional groups. *Progress in Oceanography*, *84*(1–2), 69–84. https://doi.org/10.1016/j.pocean.2009.09.008

Leonelli, F. E., Bellacicco, M., Pitarch, J., Organelli, E., Buongiorno Nardelli, B., de Toma, V., et al. (2022). Ultra-oligotrophic waters expansion in the North Atlantic Subtropical Gyre revealed by 21 years of satellite observations. *Geophysical Research Letters*, *49*(21), e2021GL096965. https://doi.org/10.1029/2021GL096965

Li, G., Cheng, L., Zhu, J., Trenberth, K. E., Mann, M. E., & Abraham, J. P. (2020). Increasing ocean stratification over the past half-century. *Nature Climate Change*, *10*(12), 1116–1123. https://doi.org/10.1038/s41558-020-00918-2

Long, J., Fassbender, A., & Estapa, M. (2021). Depth-resolved net primary production in the Northeast Pacific ocean: A comparison of satellite and profiling float estimates in the context of two marine heatwaves. *Geophysical Research Letters*, *48*(19), e2021GL093462. https://doi.org/10.1029/2021GL093462

Martínez, J., Leonelli, F. E., García-Ladona, E., Garrabou, J., Kersting, D. K., Bensoussan, N., & Pisano, A. (2023). Evolution of marine heatwaves in warming seas: The Mediterranean Sea case study. *Frontiers in Marine Science*, *10*, 1193164. https://doi.org/10.3389/fmars.2023.1193164

Marty, J.-C., Chiavérini, J., Pizay, M.-D., & Avril, B. (2002). Seasonal and interannual dynamics of nutrients and phytoplankton pigments in the western Mediterranean Sea at the DYFAMED time-series station (1991–1999). *Deep Sea Research Part II: Topical Studies in Oceanography*, *49*(11), 1965–1985. https://doi.org/10.1016/S0967-0645(02)00022-X

Marullo, S., Serva, F., Iacono, R., Napolitano, E., di Sarra, A., Meloni, D., et al. (2023). Record-breaking persistence of the 2022/23 marine heatwave in the Mediterranean Sea. *Environmental Research Letters*, *18*(11), 114041. https://doi.org/10.1088/1748-9326/ad02ae

Mayot, N., D'Ortenzio, F., Taillandier, V., Prieur, L., De Fommervault, O. P., Claustre, H., et al. (2017). Physical and biogeochemical controls of the phytoplankton blooms in North western Mediterranean Sea: A multiplatform approach over a complete annual cycle (2012–2013 DEWEX experiment). *Journal of Geophysical Research: Oceans*, *122*(12), 9999–10019. https://doi.org/10.1002/2016JC012052

Merchant, C. J., Embury, O., Bulgin, C. E., Block, T., Corlett, G. K., Fiedler, E., et al. (2019). Satellite-based time-series of sea-surface temperature since 1981 for climate applications. *Scientific Data*, *6*(1), 223. https://doi.org/10.1038/s41597-019-0236-x

Mignot, A., Claustre, H., Uitz, J., Poteau, A., D'Ortenzio, F., & Xing, X. (2014). Understanding the seasonal dynamics of phytoplankton biomass and the deep chlorophyll maximum in oligotrophic environments: A bio-Argo float investigation. *Global Biogeochemical Cycles*, *28*(8), 856–876. https://doi.org/10.1002/2013GB004781

Mignot, A., Ferrari, R., & Claustre, H. (2018). Floats with bio-optical sensors reveal what processes trigger the North Atlantic bloom. *Nature Communications*, *9*(1), 190. https://doi.org/10.1038/s41467-017-02143-6

Morán, X. A. G., López-Urrutia, A., Calvo-Díaz, A., & Li, W. K. (2010). Increasing importance of small phytoplankton in a warmer ocean. *Global Change Biology*, *16*(3), 1137–1144. https://doi.org/10.1111/j.1365-2486.2009.01960.x

Oliver, E. C., Benthuysen, J. A., Darmaraki, S., Donat, M. G., Hobday, A. J., Holbrook, N. J., et al. (2021). Marine heatwaves. *Annual Review of Marine Science*, *13*(1), 313–342. https://doi.org/10.1146/annurev-marine-032720-095144

Organelli, E., Barbieux, M., Claustre, H., Schmechtig, C., Poteau, A., Bricaud, A., et al. (2017). Two databases derived from BGC-Argo float measurements for marine biogeochemical and bio-optical applications. *Earth System Science Data*, *9*(2), 861–880. https://doi.org/10.5194/essd-9-861-2017

Organelli, E., Claustre, H., Bricaud, A., Schmechtig, C., Poteau, A., Xing, X. G., et al. (2016). A novel near-real-time quality-control procedure for radiometric profiles measured by bio-Argo floats: Protocols and performances. *Journal of Atmospheric and Oceanic Technology*, *33*(5), 937–951. https://doi.org/10.1175/Jtech-D-15-0193.1

Organelli, E., Leymarie, E., Zielinski, O., Uitz, J., D'Ortenzio, F., & Claustre, H. (2021). Hyperspectral radiometry on biogeochemical-argo floats: A bright perspective for phytoplankton diversity. *Oceanography*, *34*(4), 90–91. https://doi.org/10.5670/oceanog.2021.supplement.02-33

Organelli, E., Nuccio, C., Lazzara, L., Uitz, J., Bricaud, A., & Massi, L. (2017). On the discrimination of multiple phytoplankton groups from light absorption spectra of assemblages with mixed taxonomic composition and variable light conditions. *Applied Optics*, *56*(14), 3952–3968. https://doi.org/10.1364/AO.56.003952

Pisano, A., Marullo, S., Artale, V., Falcini, F., Yang, C., Leonelli, F. E., et al. (2020). New evidence of Mediterranean climate change and variability from sea surface temperature observations. *Remote Sensing*, *12*(1), 132. https://doi.org/10.3390/rs12010132

Ratnarajah, L., Abu-Alhaija, R., Atkinson, A., Batten, S., Bax, N. J., Bernard, K. S., et al. (2023). Monitoring and modelling marine zooplankton in a changing climate. *Nature Communications*, *14*(1), 564. https://doi.org/10.1038/s41467-023-36241-5

Rodrigues, R. R., Taschetto, A. S., Sen Gupta, A., & Foltz, G. R. (2019). Common cause for severe droughts in South America and marine heatwaves in the South Atlantic. *Nature Geoscience*, *12*(8), 620–626. https://doi.org/10.1038/s41561-019-0393-8

Sammartino, M., Di Cicco, A., Marullo, S., & Santoleri, R. (2015). Spatio-temporal variability of micro-nano-and pico-phytoplankton in the Mediterranean Sea from satellite ocean colour data of SeaWiFS. *Ocean Science*, *11*(5), 759–778. https://doi.org/10.5194/os-11-759-2015

Santoleri, R., Banzon, V., Marullo, S., Napolitano, E., D'Ortenzio, F., & Evans, R. (2003). Year-to-year variability of the phytoplankton bloom in the southern Adriatic Sea (1998–2000): Sea-viewing Wide Field-of-view Sensor observations and modeling study. *Journal of Geophysical Research*, *108*(C9), 8122. https://doi.org/10.1029/2002JC001636

Schmechtig, C., Claustre, H., Poteau, A., & D'Ortenzio, F. (2018). Bio-Argo quality control manual for the Chlorophyll-A concentration [Report]. *Argo data management*. https://doi.org/10.13155/35385

Schmechtig, C., Poteau, A., Claustre, H., D'Ortenzio, F., Dall'Olmo, G., & Boss, E. (2018). Processing BGC-Argo particle backscattering at the DAC level [Report]. *Argo data management*. https://doi.org/10.13155/39459

Smale, D. A., Wernberg, T., Oliver, E. C., Thomsen, M., Harvey, B. P., Straub, S. C., et al. (2019). Marine heatwaves threaten global biodiversity and the provision of ecosystem services. *Nature Climate Change*, *9*(4), 306–312. https://doi.org/10.1038/s41558-019-0412-1

Smith, K. E., Burrows, M. T., Hobday, A. J., King, N. G., Moore, P. J., Sen Gupta, A., et al. (2023). Biological impacts of marine heatwaves. *Annual Review of Marine Science*, *15*(1), 119–145. https://doi.org/10.1146/annurev-marine-032122-121437

Soulié, T., Vidussi, F., Mas, S., & Mostajir, B. (2022). Functional stability of a coastal Mediterranean plankton community during an experimental marine heatwave. *Frontiers in Marine Science*, *9*, 831496. https://doi.org/10.3389/fmars.2022.831496

Stoer, A. C., Takeshita, Y., Maurer, T. L., Demeaux, C. B., Bittig, H. C., Boss, E., et al. (2023). A census of quality-controlled biogeochemical-Argo float measurements. *Frontiers in Marine Science*, *10*, 1233289. https://doi.org/10.3389/fmars.2023.1233289

Thomson, J. A., Burkholder, D. A., Heithaus, M. R., Fourqurean, J. W., Fraser, M. W., Statton, J., & Kendrick, G. A. (2015). Extreme temperatures, foundation species, and abrupt ecosystem change: An example from an iconic seagrass ecosystem. *Global Change Biology*, *21*(4), 1463–1474. https://doi.org/10.1111/gcb.12694

Titaud, O., Conchon, A., & Mérillet, L. (2023). *Product user manual: For the global ocean low and mid trophic levels biomass content Hindcast product*. EU Copernicus Marine Service. https://doi.org/10.48670/moi-00020

Titaud, O., Conchon, A., Mérillet, L., & Goeman, N. (2023). *Quality information document for global MFC products (GLOBAL_-MULTIYEAR_BGC_001_033)*. EU Copernicus Marine Service. Retrieved from https://catalogue.marine.copernicus.eu/documents/QUID/CMEMS-GLO-QUID-001-033.pdf

Trainer, V. L., Moore, S. K., Hallegraeff, G., Kudela, R. M., Clement, A., Mardones, J. I., & Cochlan, W. P. (2020). Pelagic harmful algal blooms and climate change: Lessons from nature's experiments with extremes. *Harmful Algae*, *91*, 101591. https://doi.org/10.1016/j.hal.2019.03.009

Uitz, J., Stramski, D., Gentili, B., D'Ortenzio, F., & Claustre, H. (2012). Estimates of phytoplankton class-specific and total primary production in the Mediterranean Sea from satellite ocean color observations. *Global Biogeochemical Cycles*, *26*(2), GB2024. https://doi.org/10.1029/2011GB004055

Volpe, G., Buongiorno Nardelli, B., Cipollini, P., Santoleri, R., & Robinson, I. S. (2012). Seasonal to interannual phytoplankton response to physical processes in the Mediterranean Sea from satellite observations. *Remote Sensing of Environment*, *117*, 223–235. https://doi.org/10.1016/j.rse.2011.09.020

Wernberg, T., de Bettignies, T., Joy, B. A., & Finnegan, P. M. (2016). Physiological responses of habitat-forming seaweeds to increasing temperatures. *Limnology & Oceanography*, *61*(6), 2180–2190. https://doi.org/10.1002/lno.10362

Wong, A., Keeley, R., & Carval, T., & Argo Data Management Team. (2023). Argo quality control manual for CTD and trajectory data. https://doi.org/10.13155/33951

Wyatt, A. M., Resplandy, L., & Marchetti, A. (2022). Ecosystem impacts of marine heat waves in the Northeast Pacific. *Biogeosciences*, *19*(24), 5689–5705. https://doi.org/10.5194/bg-19-5689-2022

Xi, H., Losa, S. N., Mangin, A., Garnesson, P., Bretagnon, M., Demaria, J., et al. (2021). Global chlorophyll a concentrations of phytoplankton functional types with detailed uncertainty assessment using multisensor ocean color and sea surface temperature satellite products. *Journal of Geophysical Research: Oceans*, *126*(5), e2020JC017127. https://doi.org/10.1029/2020JC017127

Xi, H., Losa, S. N., Mangin, A., Soppa, M. A., Garnesson, P., Demaria, J., et al. (2020). Global retrieval of phytoplankton functional types based on empirical orthogonal functions using CMEMS GlobColour merged products and further extension to OLCI data. *Remote Sensing of Environment*, *240*, 111704. https://doi.org/10.1016/j.rse.2020.111704

Zhang, Y., Du, Y., Feng, M., & Hobday, A. J. (2023). Vertical structures of marine heatwaves. *Nature Communications*, *14*(1), 6483. https://doi.org/10.1038/s41467-023-42219-0